THE HAWAII GEOTHERMAL PROJECT

NUMERICAL SOLUTIONS FOR STEADY FREE CONVECTION IN ISLAND GEOTHERMAL RESERVOIRS

TECHNICAL REPORT No. 8

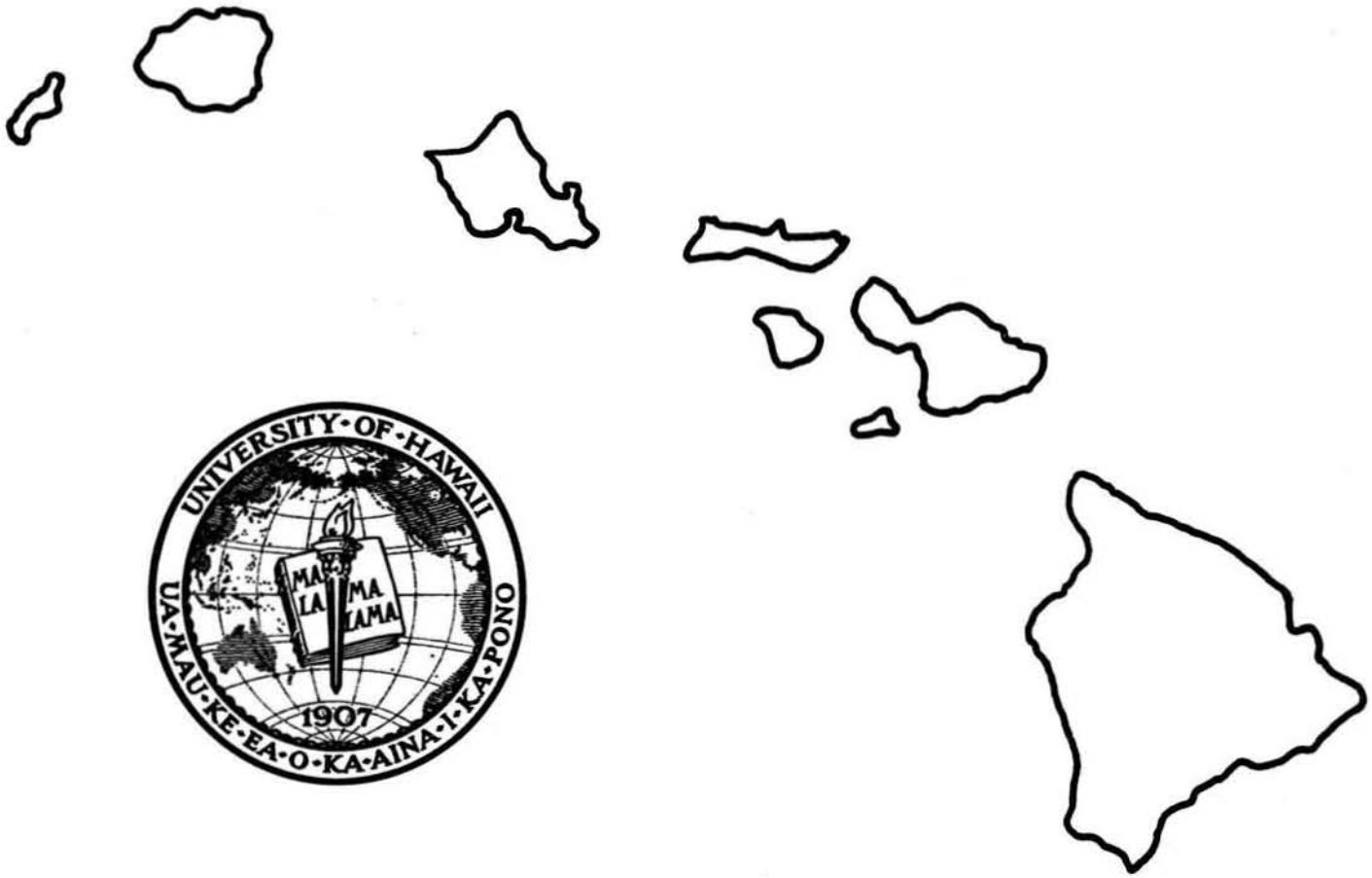

HAWAII GEOTHERMAL PROJECT

ENGINEERING PROGRAM

NUMERICAL SOLUTIONS FOR STEADY FREE CONVECTION IN ISLAND GEOTHERMAL RESERVOIRS

TECHNICAL REPORT NO. 8

August 1975

Presented at

1975 INTERNATIONAL SEMINAR ON FUTURE ENERGY PRODUCTION--
HEAT AND MASS TRANSFER PROBLEMS
Dubrovnik, Yugoslavia
August 25-30, 1975

Prepared Under

NATIONAL SCIENCE FOUNDATION
Research Grant No. GI-38319

and

ENERGY RESEARCH AND DEVELOPMENT ADMINISTRATION
Research Grant No. E(04-3)-1093

By

Ping Cheng
K. C. Yeung
and
K. H. Lau

Hilo College
University of Hawaii
Hilo, Hawaii 96720

College of Engineering
University of Hawaii
Honolulu, Hawaii 96822

NUMERICAL SOLUTIONS FOR STEADY FREE CONVECTION IN ISLAND GEOTHERMAL RESERVOIRS

PING CHENG and K. C. YEUNG
Department of Mechanical Engineering
University of Hawaii, Honolulu, Hawaii, U.S.A. 96822

K. H. LAU
Hilo College
University of Hawaii, Hilo, Hawaii, U.S.A. 96720

ABSTRACT

The problem of steady free convection in an island aquifer, confined by caprock at the top and heated by an impermeable surface from below is considered. The governing non-linear partial differential equations are approximated by a set of finite difference equations, which are solved numerically by the iteration method. To guarantee convergence of the iteration process, the non-linear convective terms in the energy equation are approximated by the upwind difference scheme. The effects of thermal conditions at the caprock, the geometry of the reservoir, the variation of Rayleigh number, the length of the heating surface, and the magmatic intrusion, on fluid flow and heat transfer characteristics in island geothermal reservoirs are discussed.

NOMENCLATURE

c_p	specific heat at constant pressure
$\bar{g}$	gravitational acceleration
h	depth of the reservoir
K	permeability of the rock
k_m	thermal conductivity of the rock
L	dimensionless width of the reservoir, $L = \ell/h$
ℓ	width of the reservoir
M	number of vertical grid lines
N	number of horizontal grid lines
p	pressure of the fluid
$\dot{Q}$	dimensionless total heat transfer rate at the bottom impermeable surface
$\dot{q}$	dimensional total heat transfer rate at the bottom impermeable surface
R	dimensionless coordinate of the axisymmetric reservoir, $R \equiv r/h$
r	coordinate of the axisymmetric reservoir
Ra	modified Rayleigh number, $Ra \equiv \rho_s g h K \beta (T_m - T_s)/\alpha\mu$

T temperature of the fluid

T_a temperature of the caprock

T_d temperature of the intrusive

T_m maximum temperature of the impermeable surface

U dimensionless horizontal velocity, $U \equiv u\mu/\rho_s g\beta(T_m-T_s)K$

u horizontal velocity

V dimensionless vertical velocity, $V = v\mu/\rho_s g\beta(T_m-T_s)K$

v vertical velocity

Z dimensionless coordinate

z dimensional coordinate

Greek symbols

α equivalent thermal diffusivity, $\alpha \equiv k_m/(\rho C_p)_f$

β thermal expansion coefficient of the fluid

γ relaxation factor defined in Eq. (25b)

ε error tolerance, defined in Eq. (26)

θ dimensionless temperature, $\theta \equiv (T-T_s)/(T_m-T_s)$

θ_a, θ_d, θ_L, θ_s dimensionless temperatures

λ defined in Eq. (18a)

μ viscosity of the fluid

ρ density of the fluid

Ψ dimensionless stream function

ψ dimensional stream function

ω relaxation factor defined in Eq. (25a)

Superscript

$*$ temporary values of θ and Ψ

Subscript

s condition in the ocean

The rapid depletion of the reserves of fossil fuels has stimulated considerable interest in the utilization of geothermal energy for power generation. Depending on geological and hydrological conditions, the geothermal resources that can be utilized for power production with the present technology exist in the form of hot water or steam in the earth's crust. It has been postulated by geologists that, as a result of heating from hot rocks, groundwater adjacent to the heated rock will rise to the top of the aquifer [1]. If the aquifer is confined by caprock with poor thermal conductivity which prevents the dissipation of heat, a large amount of hot fluids at relatively shallow depths could be available for power generation. Thus an ideal reservoir for geothermal energy extraction would consist of a hot heat source for the continuous supply of energy, a highly permeable aquifer to permit the free flow of a large amount of groundwater, and a poor heat conducting caprock for the storage of heat.

The proposed mechanism by which heat is transferred from deep igneous rocks to groundwater at shallow depths in geothermal areas has been supported quantitatively by a number of theoretical studies. Wooding [2] appears to be the first to study the non-linear problem of free convection in confined reservoirs. In Wooding's analysis, a perturbation method was used to approximate the governing non-linear partial differential equations by a set of linear subproblems which can be solved numerically. Using a two-layer model consisting of an upper saturated permeable layer and an underlying layer of impermeable basement, Donaldson [3] obtained a finite difference solution to steady free convection in a confined reservoir. Numerical solutions were also obtained by Elder [4,5] who studied the roles of end effects, non-uniform heating, and mass discharge on steady and transient free convection in bounded rectangular reservoirs with a small aspect (height to width) ratio. The effect of through flow on the local circulatory flow in reservoirs with large aspect ratio was treated numerically by Donaldson [6]. The effects of geothermal heating of saline groundwater in a coastal aquifer with application to waste disposal was studied by Henry and Kohout [7], using the finite difference method. The simulation of the confined geothermal reservoir at Wairakei, New Zealand, taking into consideration the irregular geometry, was performed by Mercer [8] on the basis of the finite element method. Most recently, a variation of Wooding's perturbation method was applied by Cheng and Lau [9] to study free convection in unconfined geothermal reservoirs at low Rayleigh numbers.

In this paper, we shall study the effects of (i) thermal conditions at the caprock, (ii) the geometry of the reservoir, (iii) the variation of Rayleigh number, (iv) the size of the heating surface, and (v) the magmatic intrusion on the fluid flow and heat transfer characteristics in an island aquifer (Fig. 1). To simplify the problem, idealized models shown in Fig. 2 will be treated. The set of non-linear governing equations are approximated by a set of finite difference equations, which are solved by Gauss-Seidel iteration method. To guarantee convergence the non-linear convective terms are approximated by the upwind difference scheme [11]. The over- and under-relaxation methods are incorporated in a "combined iteration" procedure [11] to accelerate the rate of convergence. Streamlines, isotherms, and velocity distribution for cylindrical and rectangular reservoirs at a selected set of parameters are presented.

FORMULATION OF THE PROBLEM

In the mathematical formulation of the problem, the following assumptions will be made:

1) The flow and temperature fields are steady.
2) The groundwater and the porous rock are in local thermodynamic equilibrium.
3) The temperature of the fluid is everywhere below boiling for the

pressure at that depth.

4) Boussinesq approximation is employed.

The governing equations for the simultaneous heat and mass transfer in a saturated porous medium are the continuity equation, Darcy's Law, energy equation, and equation of state which are given by

$$\text{div } \bar{v} = 0 , \tag{1}$$

$$\bar{v} = -\frac{K}{\mu}(\nabla p - \rho\bar{g}) , \tag{2}$$

$$\bar{v}\cdot\nabla T = \alpha\nabla^2 T , \tag{3}$$

$$\rho = \rho_s[1 - \beta(T-T_s)] , \tag{4}$$

where $\bar{v}$, ρ, μ and β are the macroscopic velocity vector, density, viscosity and the thermal expansion coefficient of the fluid, p the pressure, T the temperature, g the gravitational acceleration. $\alpha = k_m/(\rho C_p)_f$ is the equivalent thermal diffusivity with k_m denoting the thermal conductivity of the porous medium and $(\rho C_p)_f$ the density and specific heat of the fluid. The subscript s in Eq. (4) denotes the condition in the ocean.

In this paper, we shall consider free convective flow in both cylindrical and rectangular geothermal reservoirs. Consider, first, an axisymmetric reservoir as shown in Fig. 2A. It can be shown that Eqs. (1)-(4) can be written in the following dimensionless form

$$\frac{\partial^2\Psi}{\partial R^2} - \frac{1}{R}\frac{\partial\Psi}{\partial R} + \frac{\partial^2\Psi}{\partial Z^2} = R\frac{\partial\theta}{\partial R} , \tag{5}$$

and

$$\frac{\partial^2\theta}{\partial R^2} + \frac{1}{R}\frac{\partial\theta}{\partial R} + \frac{\partial^2\theta}{\partial Z^2} = \frac{Ra}{R}\left(\frac{\partial\Psi}{\partial R}\frac{\partial\theta}{\partial Z} - \frac{\partial\Psi}{\partial Z}\frac{\partial\theta}{\partial R}\right) , \tag{6}$$

where $R \equiv r/h$, $Z \equiv z/h$, and $\theta \equiv (T-T_s)/(T_m-T_s)$ with T_m denoting the maximum temperature of the impermeable surface. The dimensionless stream function in Eqs. (5) and (6) is defined in the usual manner, i.e., $U = (1/R)(\partial\Psi/\partial Z)$ and $V = -(1/R)(\partial\Psi/\partial R)$ where $\Psi \equiv \psi\mu/\rho_s g h^2 K\beta(T_m-T_s)$, $U \equiv u\mu/\rho_s g\beta(T_m-T_s)K$, and $V \equiv v\mu/\rho_s g\beta(T_m-T_s)K$ with ψ, u, and v denoting the dimensional stream function and velocity components. The parameter Ra in Eq. (6) is defined as $Ra \equiv \rho_s g h K\beta(T_m-T_s)/\alpha\mu$ which is the modified Rayleigh number.

The appropriate boundary conditions for an axisymmetric aquifer, bounded by ocean on the side, confined by caprock at the top, and heated by a horizontal impermeable surface at the bottom with a prescribed temperature $T_L(R)$, are

$$\Psi(R,0) = 0 , \qquad \theta(R,0) = \theta_L(R) , \tag{7}$$

$$\frac{\partial\Psi}{\partial R}\left(\frac{L}{2}, Z\right) = 0 , \qquad \theta\left(\frac{L}{2}, Z\right) = 0 , \tag{8}$$

$$\Psi(0,Z) = 0 , \qquad \frac{\partial\theta}{\partial R}(0,Z) = 0 , \tag{9}$$

$$\Psi(R,1) = 0 , \tag{10}$$

where $\theta_L(R) \equiv (T_L-T_s)/(T_m-T_s)$. In addition, the following two thermal boundary conditions at the caprock will be considered.

(1) a heat conducting caprock with temperature T_a, the boundary condition is

$$\theta(R,1) = \theta_a \text{ , or} \qquad (11a)$$

(2) an adiabatic caprock, with the boundary condition given by

$$\frac{\partial\theta}{\partial Z}(R,1) = 0 \text{ ,} \qquad (11b)$$

where $\theta_a \equiv (T_a-T_s)/(T_m-T_s)$. If a hot impermeable intrusive is located at the center of the aquifer, the additional boundary conditions are $\Psi=0$, and $\theta=\theta_d$ along its impermeable surface where $\theta_d \equiv (T_d-T_s)/(T_m-T_s)$ with T_d denoting the temperature of the intrusive.

The corresponding equations for a two-dimensional rectangular reservoir shown in Fig. 2B are

$$\frac{\partial^2\Psi}{\partial X^2} + \frac{\partial^2\Psi}{\partial Z^2} = -\frac{\partial\theta}{\partial X} \text{ ,} \qquad (12)$$

$$\frac{\partial^2\theta}{\partial X^2} + \frac{\partial^2\theta}{\partial Z^2} = Ra\left(\frac{\partial\Psi}{\partial Y}\frac{\partial\theta}{\partial X} - \frac{\partial\Psi}{\partial X}\frac{\partial\theta}{\partial Y}\right) \text{ ,} \qquad (13)$$

where $X \equiv x/h$ and $\Psi \equiv \mu\psi/\rho_s g h \beta (T_m-T_s)K$ which is related to the dimensionless velocity components by $U = \partial\Psi/\partial Z$ and $V = -\partial\Psi/\partial X$. The appropriate boundary conditions for a rectangular reservoir is also given by Eqs. (7)-(11) with R replaced by X.

FINITE DIFFERENCE EQUATIONS AND NUMERICAL SOLUTIONS

In this section, we shall confine our attention to the numerical solution for free convection in a cylindrical aquifer. The corresponding problem for a rectangular aquifer can be done in a similar fashion (see Ref. [10]). Since the problem is symmetric with respect to z axis, we only need to consider half of the domain as shown in Fig. 3. We first superimpose a rectangular grid on the domain with the coordinates of the grid points given by (R_i,Z_j) where $R_i=(i-1)\Delta R(i=1,2,\ldots,M)$ and $Z_j=(j-1)\Delta Z(j=1,2,\ldots,N)$. To obtain the finite difference equations, the standard five point formula is applied to Eqs. (5) and (6). The first derivatives in the linear terms in the equations are approximated by central difference whereas the first derivative for θ in each of the non-linear terms is approximated by the upwind difference scheme [11], whereby the forward or backward finite difference approximations are used depending upon whether the local velocity component is positive or negative. As a result of this difference scheme, the coefficient matrix for θ is diagonally dominant which would guarantee convergence if the Gauss-Seidel iteration method is used. Thus, for an interior node in a cylindrical aquifer, the finite difference equations are

$$\frac{\Psi_{i+1,j} - 2\Psi_{i,j} + \Psi_{i-1,j}}{(\Delta R)^2} - \frac{1}{\Delta R(i-1)}\frac{\Psi_{i+1,j} - \Psi_{i-1,j}}{2\Delta R} +$$

$$\frac{\Psi_{i,j+1} - 2\Psi_{i,j} + \Psi_{i,j-1}}{(\Delta Z)^2} = (i-1)\Delta R\,\frac{\theta_{i+1,j} - \theta_{i-1,j}}{2\Delta R} \text{ ,} \qquad (14)$$

and

$$\frac{\theta_{i+1,j} - 2\theta_{i,j} + \theta_{i-1,j}}{(\Delta R)^2} + \frac{1}{\Delta R(i-1)} + \frac{\theta_{i,j+1} - 2\theta_{i,j} + \theta_{i,j-1}}{(\Delta Z)^2}$$

$$= Ra \left\{ U_{i,j} \left(\frac{A_1\theta_{i+1,j} + A_2\theta_{i,j} + A_3\theta_{i-1,j}}{\Delta R} \right) + \right.$$

$$\left. V_{i,j} \left(\frac{A_4\theta_{i,j+1} + A_5\theta_{i,j} + A_6\theta_{i,j-1}}{\Delta Z} \right) \right\}, \qquad (15)$$

which can be solved for $\Psi_{i,j}$ and $\theta_{i,j}$ to give

$$\psi^{*(k+1)}_{i,j} = \frac{1}{2(1+\lambda^2)} \left\{ \left[1 - \frac{1}{2(i-1)}\right]\psi^{(k)}_{i+1,j} + \left[1 + \frac{1}{2(i-1)}\right]\psi^{(k)}_{i-1,j} \right.$$

$$\left. + \lambda^2[\psi^{(k)}_{i,j+1} + \psi^{(k)}_{i,j-1}] - (i-1)(\Delta R)^2 \frac{\theta^{(k)}_{i+1,j} - \theta^{(k)}_{i-1,j}}{2} \right\}, \qquad (16)$$

and

$$\theta^{*(k+1)}_{i,j} = \frac{1}{[2(1+\lambda^2) + RaU^{(k+1)}_{i,j}A_2(\Delta R) + RaV^{(k+1)}_{i,j}A_5(\Delta R)]} \left\{ \left[1 + \frac{1}{2(i-1)} - \right.\right.$$

$$RaU^{(k+1)}_{i,j}A_1(\Delta R)\Big]\theta^{(k)}_{i+1,j} + \left[1 - \frac{1}{2(i-1)} + RaU^{(k+1)}_{i,j}A_3(\Delta R)\right]\theta^{(k)}_{i-1,j} +$$

$$\left. \left[\lambda^2 - RaV^{(k+1)}_{i,j}A_6(\Delta R)\lambda\right]\theta^{(k)}_{i,j-1} + \left[\lambda^2 - RaV^{(k+1)}_{i,j}A_4(\Delta R)\lambda\right]\theta^{(k)}_{i,j+1} \right\}, \qquad (17)$$

where

$$\lambda \equiv \frac{\Delta R}{\Delta Z}, \qquad (18a)$$

$$U^{(k+1)}_{i,j} = \frac{\psi^{(k+1)}_{i+1,j} - \psi^{(k+1)}_{i-1,j}}{2(i-1)\Delta R\Delta Z}, \qquad (18b)$$

$$V^{(k+1)}_{i,j} = \frac{\psi^{(k+1)}_{i,j+1} - \psi^{(k+1)}_{i,j-1}}{2(i-1)(\Delta R)^2}, \qquad (18c)$$

and

$$A_1 = 0, \quad A_2 = 1, \quad A_3 = -1, \quad \text{when } U_{i,j} \geq 0, \qquad (19a)$$

$$A_4 = 0, \quad A_5 = 1, \quad A_6 = -1, \quad \text{when } V_{i,j} \geq 0, \qquad (19b)$$

$$A_1 = 1, \quad A_2 = -1, \quad A_3 = 0, \quad \text{when } U_{i,j} < 0, \qquad (19c)$$

$$A_4 = 1, \quad A_5 = -1, \quad A_6 = 0, \quad \text{when } V_{i,j} < 0. \qquad (19d)$$

The finite difference equations for grid points along the center line R=0 (i.e. i=1) need special attention since the terms $(1/R)(\partial\Psi/\partial R)$ and $(1/R)(\partial\theta/\partial R)$ in Eq. (6) become indefinite as R→0. From l'Hospital's rule, we have

$$\lim_{R\to 0} \frac{1}{R}\frac{\partial\theta}{\partial R} = \frac{\partial^2\theta}{\partial R^2} , \tag{20a}$$

and

$$V(0,Z) = \lim_{R\to 0} \frac{1}{R}\frac{\partial\Psi}{\partial R} = \frac{\partial^2\Psi}{\partial R^2} . \tag{20b}$$

It follows that, as R→0, Eq. (6) becomes

$$2\frac{\partial^2\theta}{\partial R^2} + \frac{\partial^2\theta}{\partial Z^2} = Ra\,\frac{\partial\theta}{\partial Z}\frac{\partial^2\Psi}{\partial R^2} , \tag{21}$$

where we have made use of the condition $\partial\Psi/\partial Z = 0$ as R→0. Thus the finite difference equation corresponding to Eq. (21) is given by

$$\frac{4[\theta_{2,j} - \theta_{1,j}]}{(\Delta R)^2} + \frac{\theta_{1,j+1} - 2\theta_{1,j} + \theta_{1,j-1}}{(\Delta Z)^2} = RaV_{1,j}\left(\frac{A_4\theta_{1,j+1} + A_5\theta_{i,j} + A_6\theta_{1,j-1}}{\Delta Z}\right), \tag{22a}$$

which can be solved for $\theta_{1,j}$ to give

$$\theta_{1,j}^{(k+1)} = \frac{1}{[2(2+\lambda^2) - RaV_{1,j}^{(k+1)}\lambda\Delta RA_5]}\left\{4\theta_{2,j}^{(k)} + [\lambda^2 - RaV_{1,j}^{(k+1)}\lambda\Delta RA_4]\theta_{1,j+1}^{(k)}\right.$$

$$\left. + [\lambda^2 - RaV_{1,j}^{(k+1)}\lambda\Delta RA_6]\theta_{1,j-1}^{(k)}\right\} . \tag{22b}$$

The finite difference equations corresponding to boundary conditions (7)-(9) are

$$\Psi_{i,1} = 0 , \quad \theta_{i,1} = \theta_L(R_i) , \quad \text{for } i=1,2,\ldots,M , \tag{23a}$$

$$\Psi_{M,j} = \frac{1}{3}(4\Psi_{M-1,j} - \Psi_{M-2,j}), \quad \theta_{M,j} = \theta_s , \quad \text{for } j=1,2,\ldots,N , \tag{23b}$$

$$\Psi_{1,j} = 0 , \quad \text{for } j=1,2,\ldots,N , \tag{23c}$$

$$\Psi_{i,N} = 0 , \quad \text{for } i=1,2,\ldots,M , \tag{23d}$$

and

$$\theta_{i,N} = \theta_a , \ (i=1,2,\ldots,M) \text{ for a heat conducting caprock,} \tag{24a}$$

or

$$\theta_{i,N} = \frac{1}{3}(4\theta_{i,N-1} - \theta_{i,N-2}) \text{ for an adiabatic caprock,} \tag{24b}$$

where we have used the three point formula for the derivative boundary conditions in Eqs. (23b) and (24b).

We now describe the "combined" iteration procedures [11] for the numerical solutions of Eqs. (16)-(19), (23) and (24).

(1) Select a value for Ra and assume the initial values of $\theta_{i,j}^{(k)}$ and $\Psi_{i,j}^{(k)}$.

(2) Find a temporary value of $\Psi_{i,j}^{*(k+1)}$ from Eq. (16).

(3) The new iteration value for $\Psi_{i,j}^{(k+1)}$ is obtained from the formula

$$\Psi_{i,j}^{(k+1)} = \Psi_{i,j}^{(k)} + \omega(\Psi_{i,j}^{*(k+1)} - \Psi_{i,j}^{(k)}) , \tag{25a}$$

where ω is called the over-relaxation factor if $1 \leq \omega \leq 2$ and under-relaxation factor if $0 \leq \omega \leq 1$.

(4) Compute $U_{i,j}^{(k+1)}$ and $V_{i,j}^{(k+1)}$ from Eqs. (18b) and (18c).

(5) Find a temporary value of $\theta_{i,j}^{*(k+1)}$ from Eq. (17).

(6) The new iteration value for $\theta_{i,j}^{(k+1)}$ is obtained from

$$\theta_{i,j}^{(k+1)} = \theta_{i,j}^{(k)} + \gamma(\theta_{i,j}^{*(k+1)} - \theta_{i,j}^{(k)}) , \tag{25b}$$

where γ is the relaxation factor.

(7) Repeat steps (2)-(6). The iteration process is terminated until the following criteria are simultaneously satisfied:

$$\left| \frac{\psi^{(k+1)} - \psi^{(k)}}{\psi_{max}^{(k+1)}} \right| < \varepsilon , \quad \left| \frac{\theta^{(k+1)} - \theta^{(k)}}{\theta_{max}^{(k+1)}} \right| < \varepsilon . \tag{26}$$

RESULTS AND DISCUSSION

Convergent results were obtained for $0 \leq Ra \leq 2000$ with $L=4$, $\varepsilon=10^{-4}$, and $\lambda=1$ ($\Delta Z=\Delta R=0.1$), where the values of ε, ΔZ, and ΔR were dictated by economic considerations. Computations were carried out for the following cases.

1. Cylindrical island aquifer with a heat conducting caprock. The prescribed temperatures for this case are: $\theta_a=\theta_s=0$, and $\theta_L(R)=\exp[-(2R)^2]$.
2. Cylindrical island aquifer with an adiabatic caprock. The prescribed temperatures for $\theta_L(R)$ and θ_s are the same as Case 1.
3. Rectangular island aquifer with a heat conducting caprock. The prescribed temperatures are $\theta_a=\theta_s=0$, with the following two cases of $\theta_L(X)$ considered:
   A. Continuous wall temperature with $\theta_L(X)=\exp[-(2X)^2]$, and
   B. Discontinuous wall temperature with $\theta_L(X)=1$ for $-f/2 \leq X \leq f/2$ (where f is the dimensionless heating length normalized with respect to h) and $\theta_L(X)=0$ elsewhere.
4. Rectangular island aquifer with an adiabatic caprock. The prescribed temperatures for $\theta_L(X)$ and θ_s are the same as Case 3A.
5. Rectangular island aquifer with dike intrusion. The magmatic intrusive, located at the center of the aquifer, is 2 units in width and 0.5 units in height. The prescribed temperatures are $\theta_a=\theta_s=0$, $\theta_d=1$, and $\theta_L(X)=1$ for $-1 \leq X \leq 1$ and $\theta_L(X)=0$ elsewhere.

Representative results of the five cases are presented in Figs. 4-19. We shall now discuss the effects of Rayleigh number, the thermal boundary conditions at the caprock, the geometry of the reservoir, the heating length, and the dike intrusion on the fluid flow and heat transfer characteristics in a geothermal reservoir.

The Effects of Rayleigh Number

Figures 4-7 and 9-10 show the fluid flow and heat transfer characteristics in a cylindrical aquifer at different values of Ra with a heat conducting caprock (i.e., Case 1). Figure 4 shows the convective pattern at two values of Ra. In both of these figures, cold sea water moves inland along the lower portion of the aquifer and is gradually heated by the impermeable surface. Near the point of maximum heating, the fluid rises upward like a thermal plume. As the hot water reaches to the top, it spreads around the caprock and is finally discharged to the ocean in the upper portion of the aquifer. A comparison of Fig. 4A and Fig. 4B shows that closed convective cells disappear as Ra is increased. The effects of Ra on the isotherms in a cylindrical island aquifer

is shown in Fig. 5. For small values of Ra (Ra=50 for example), the isotherms are similar to those by heat conduction. As the value of Ra is increased, the isotherms develop into mushroom shapes with increasing size. Similar results were obtained by Elder [4,5] for a bounded rectangular reservoir. The effect on Ra on the temperature distribution along Z = 0.2, 0.4, 0.6, and 0.8 is shown on Fig. 6. The temperature distribution is bell shaped with a maximum value at the center; the rate of increase in temperature in the region near the center is rapid for large Ra, indicating a boundary layer behavior.

The vertical temperature profiles in the aquifer are shown in Fig. 7. At low Ra vertical temperature profiles increase almost linearly with depth, indicating conduction is predominant. At higher values of Ra, where convection becomes important, vertical profile at the center of the thermal plume (i.e., R=0) differs from the rest of the profiles which have a temperature reversal at a vertical distance not too far from the caprock. The temperature reversal, which is an indication of lateral movement of warm water, is most pronounced for large Ra at a horizontal distance not far from the heat source. It is interesting to note that temperature vs depth measurements obtained by Keller [11] at the summit of Kilauea volcano also shows a temperature inversion. A comparison of the computed vertical temperature profile (at R=0.2 and Ra=2000) and with Keller's data shows a striking similarity (Fig. 8).

The effects of Ra on the vertical and horizontal profiles are shown in Figs. 9 and 10. A comparison of Figs. 9 and 6 reveals that temperature and vertical velocity are similar in shape. As shown in Fig. 9, the vertical velocity is vanishing small everywhere except in the thermal plume. The width of the thermal plume decreases as Ra is increased. The relative magnitudes of the horizontal and vertical velocity at different Ra depends on the location under consideration. At the center of the plume, the vertical velocity is maximum; its magnitude increases as Ra is increased. From the governing equations, it can be shown that the slope of the horizontal velocity profile at the wall depends only on the local temperature gradient of the wall, i.e.,

$$\left(\frac{\partial U}{\partial Z}\right)_{Z=0} = -\left(\frac{\partial \theta}{\partial R}\right)_{Z=0} .$$

It follows that, at a particular location, the horizontal temperature gradients at the wall are independent of Ra. This is confirmed by most of the profiles in Fig. 10.

Effects of Thermal Boundary Condition at the Caprock

Numerical results for Case 2 are presented in Figs. 11 and 12. A comparison of Figs. 5 and 7 to Figs. 11 and 12 shows that the adiabatic caprock acts to prevent the dissipation of heat so that a larger amount of hot water at shallow depth is available. It is interesting to note that the increase in temperature due to the adiabatic caprock is most significant in the region adjacent to the caprock. Away from the caprock, temperature of the water is relatively independent of the thermal boundary condition at the caprock. Consequently, the total dimensionless heat transfer rate at the bottom impermeable surface, $\bar{Q}$ (where $\bar{Q} = q/2\pi K_m h(T_m - T_s)$ with q denoting the dimensional heat transfer rate), is relatively independent of the thermal boundary condition at the caprock (Fig. 13). The magnitude of $\bar{Q}$ increases more than ten times from Ra = 0 to Ra = 2,000.

Effects of Geometry of the Reservoir

To show the effects of geometry of the reservoir on the fluid flow and heat transfer characteristics, the results of Cases 1 and 2 at Ra=2000 are compared with those of Cases 3A and 4 in Figs. 14-17. At a corresponding location it is seen that temperature distribution in a cylindrical aquifer is lower than that of a rectangular reservoir (Figs. 14 and 15). Furthermore, although the horizontal velocity in a rectangular aquifer is larger than that in a cylindrical aquifer at a corresponding location (Fig. 16), the vertical velocity in a rectangular aquifer is smaller than that in a cylindrical one (Fig. 17).

Effects of Heating Length

Results of Cases 3B and 5 at Ra=300 are plotted in Figs. 18 and 19 to show the effects of the size of the heating length and the dike intrusion on streamlines and isotherms in a rectangular reservoir. As in the case of a bounded aquifer, the number of convective cells depends on the heating length, with two convective cells for f = 2 (Figs. 18A and 19A) and four cells for f = 3 (Figs. 18B and 19B). The convective pattern not only depends on the heating length but also on the manner it is heated. For example, although Figs. 18B and 18C have the same heating length, the streamline patterns are completely different. A comparison of Figs. 18A and 18C as well as Figs. 19A and 19C shows that the streamlines and isotherms of the two cases are similar to each other although the reservoir with a dike (Figs. 18C and 19C) has a heating length 1/3 times longer.

ACKNOWLEDGMENT

The study is a part of the Hawaii Geothermal Project funded in part by the RANN program of the National Science Foundation of the United States (Grant No. GI-38319) and by the State and County of Hawaii.

REFERENCES

1. White, D.E., Geothermal Energy, Resources Production, Stimulation, Stanford University Press, 69-94 (1973).
2. Wooding, R.A., J.F.M., V. 2, 273-285 (1957).
3. Donaldson, I.G., J. Geophysical Research, V. 67, 3449-3459 (1962).
4. Elder, J.W., J.F.M., V. 27, 29-48 (1967).
5. Elder, J.W., J.F.M., V. 27, 609-623 (1967).
6. Donaldson, I.G., Geothermics, 649-654 (1970).
7. Henry, H.R., and Kohout, F.A., Underground Waste Manage, Environ. Implications, V. 18, 202-221 (1973).
8. Mercer, J.W., Jr., "Finite Element Approach to the Modeling of Hydrothermal Systems," Ph.D. thesis in Geology, University of Illinois at Urbana-Champaign (1973).
9. Cheng, P., and Lau, K.H., J. Geophys. Res., V. 79, 4425-4431 (1974).
10. Cheng, P., Yeung, K.C., and Lau, K.H., Hawaii Geothermal Project, Tech. Rept. No. 8 (1975).
11. Roache, P.J., Computational Fluid Dynamics, Hermosa Publishers (1972).
12. Keller, G.V., "Drilling at the Summit of Kilauea Volcano," prepared for National Science Foundation, Colorado School of Mines, Golden, Colorado, March 15, 1974.

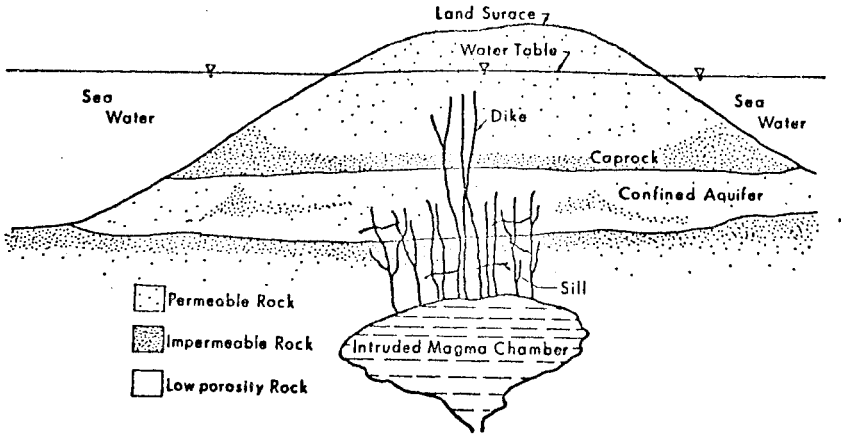

Fig. 1 Island Aquifer with Geothermal Heat Source

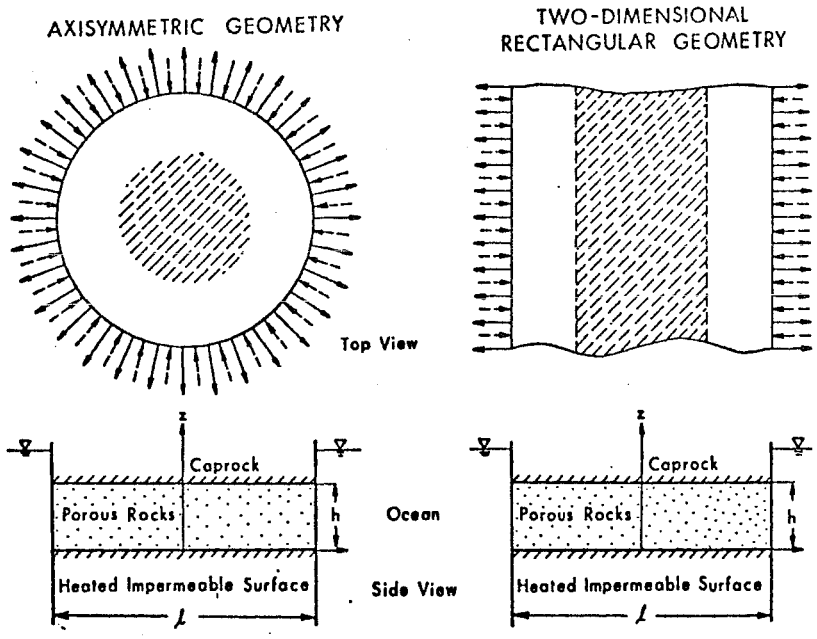

Fig. 2 Idealized Models for Free Convection in Island Geothermal Reservoirs

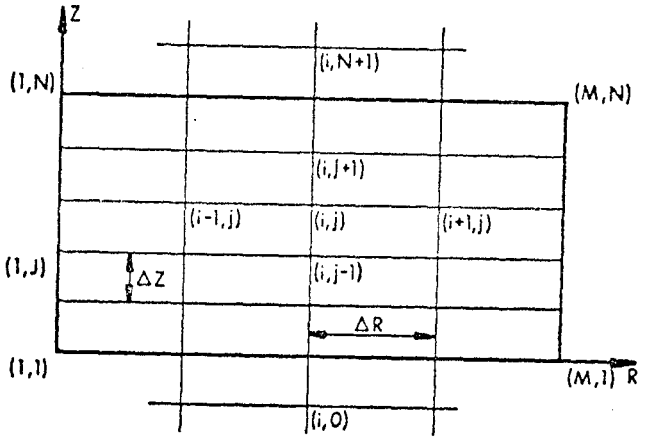

Fig. 3 Grid Points for Finite Difference Equations

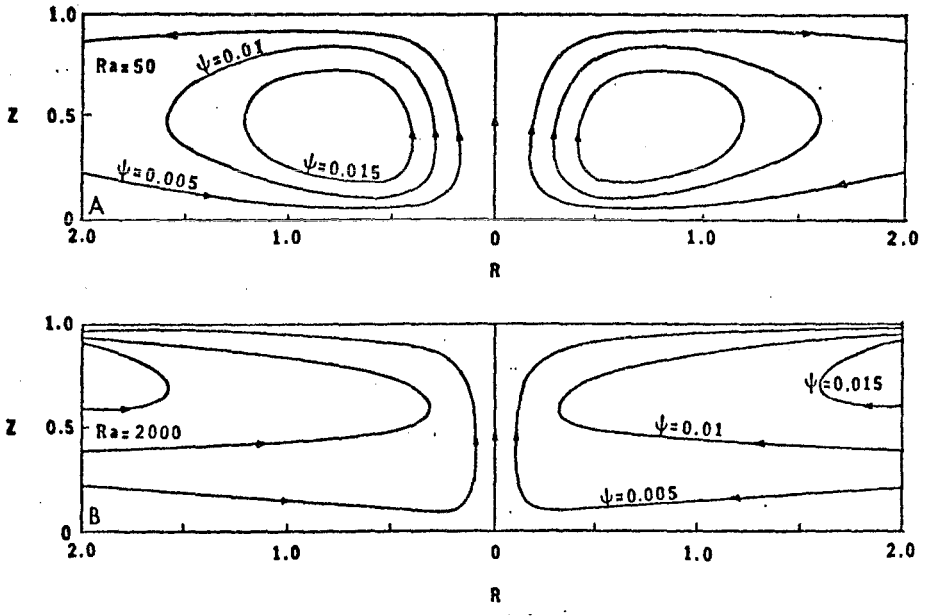

Fig. 4 The Effect of Rayleigh Number on Streamlines in an Axisymmetric Geothermal Reservoir with Heat-Conducting Caprocks

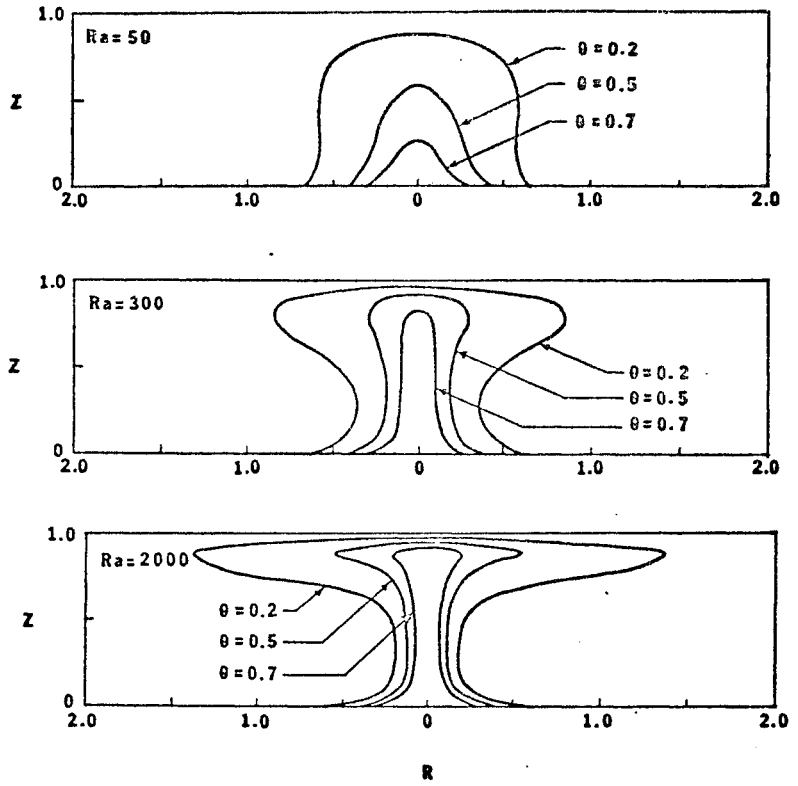

Fig. 5 The Effect of Rayleigh Number on Isotherms in an Axisymmetric Geothermal Reservoir with Heat-Conducting Caprocks

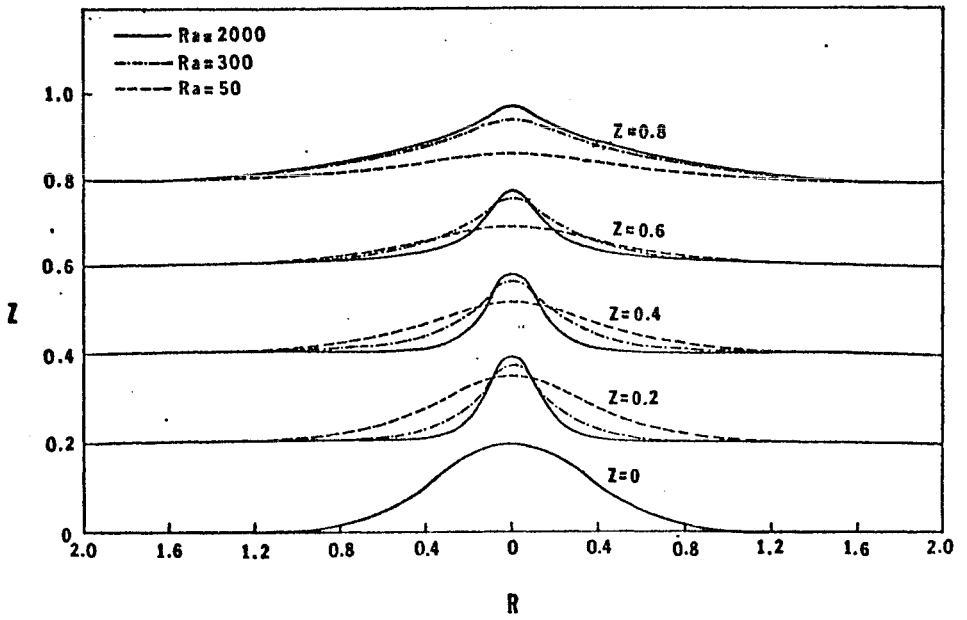

Fig. 6 The Effect of Rayleigh Number on the Horizontal Temperature Distribution in an Axisymmetric Reservoir with Heat-Conducting Caprocks

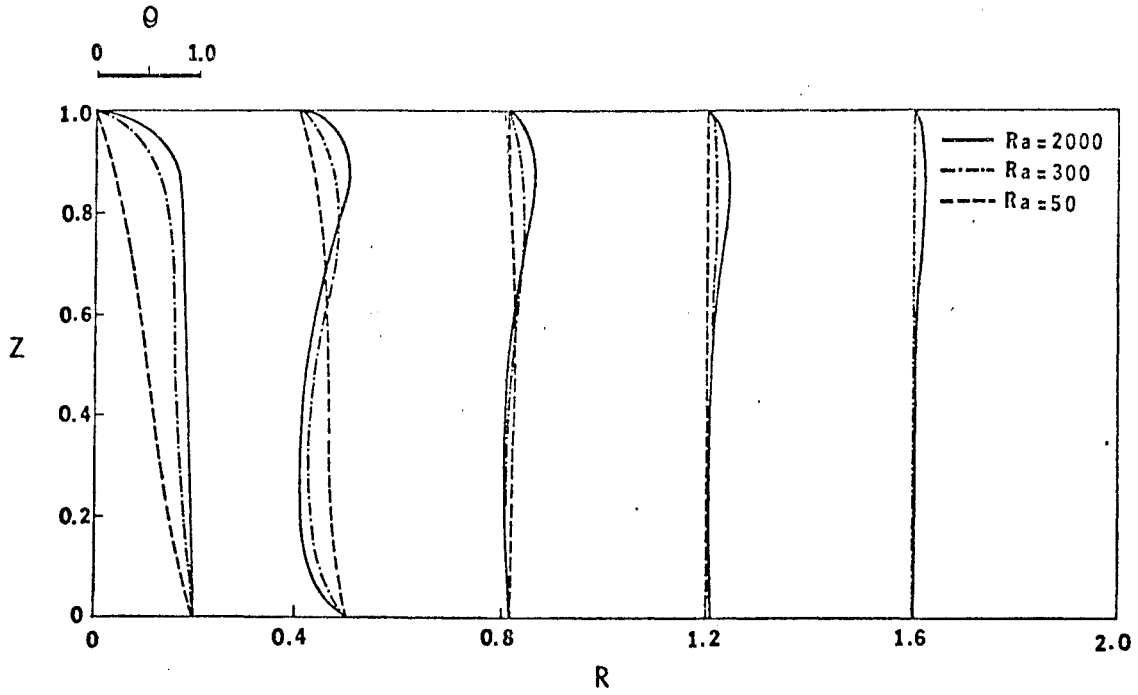

Fig. 7 The Effect of Rayleigh Number on the Vertical Temperature Profiles in an Axisymmetric Reservoir with Heat-Conducting Caprocks

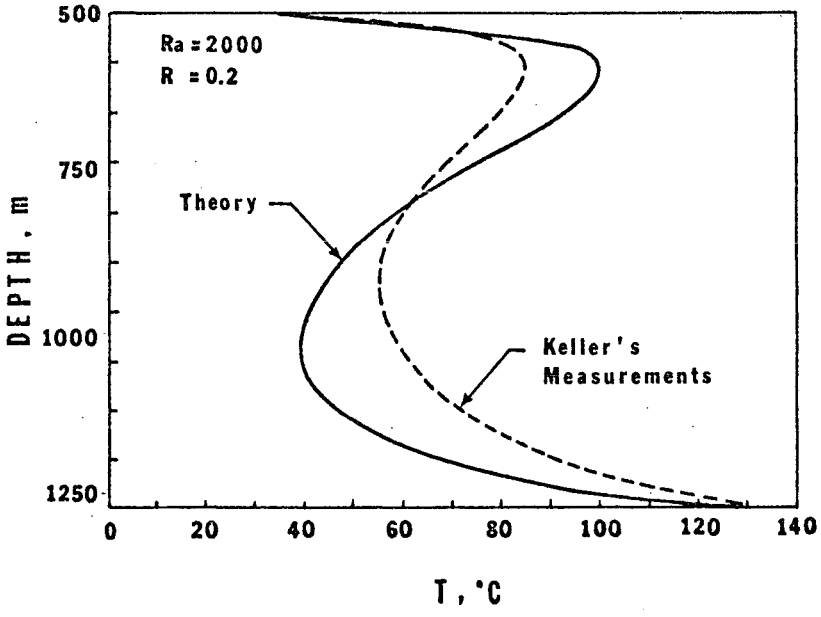

Fig. 8 Comparison of Theory and Measurement

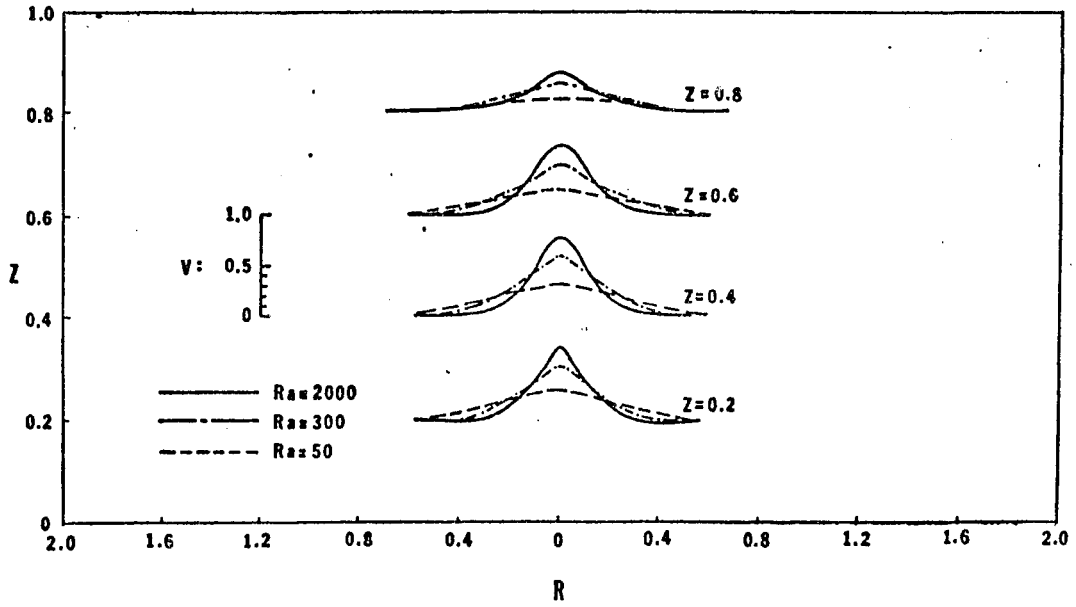

Fig. 9 The Effect of Rayleigh Number on Vertical Velocity Profiles in an Axisymmetric Reservoir with Heat-Conducting Caprocks

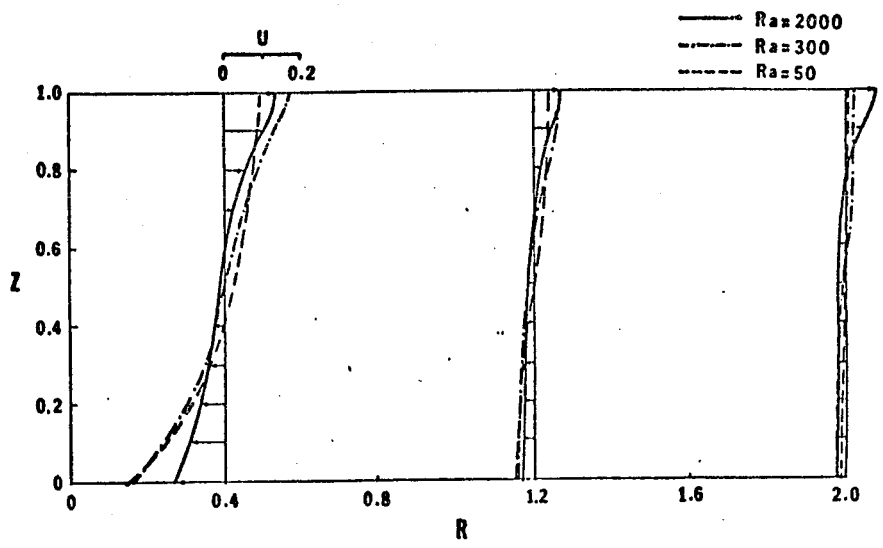

Fig. 10 The Effect of Rayleigh Number on Horizontal Velocity Profiles in an Axisymmetric Reservoir with Heat-Conducting Caprocks

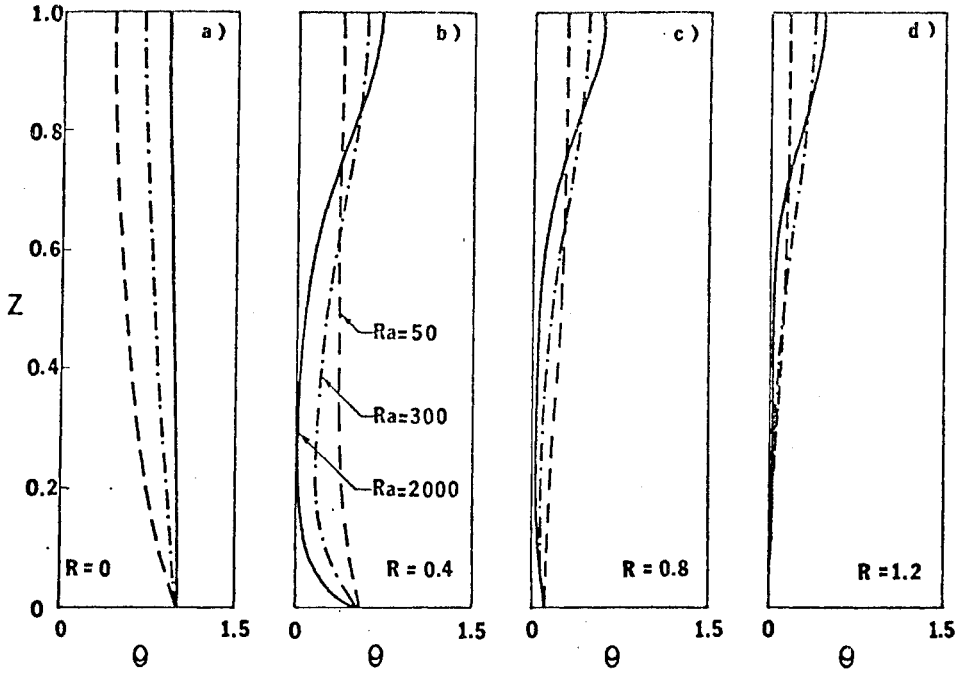

Fig. 11 The Effect of Rayleigh Number on the Vertical Temperature Profiles in an Axisymmetric Geothermal Reservoir with Adiabatic Caprocks

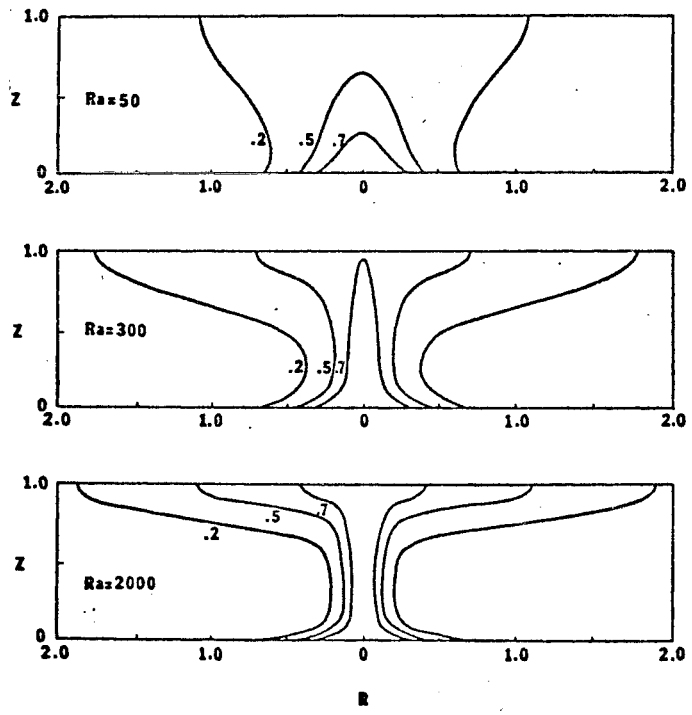

Fig. 12 The Effect of Rayleigh Number on Isotherms in an Axisymmetric Geothermal Reservoir with Adiabatic Caprocks

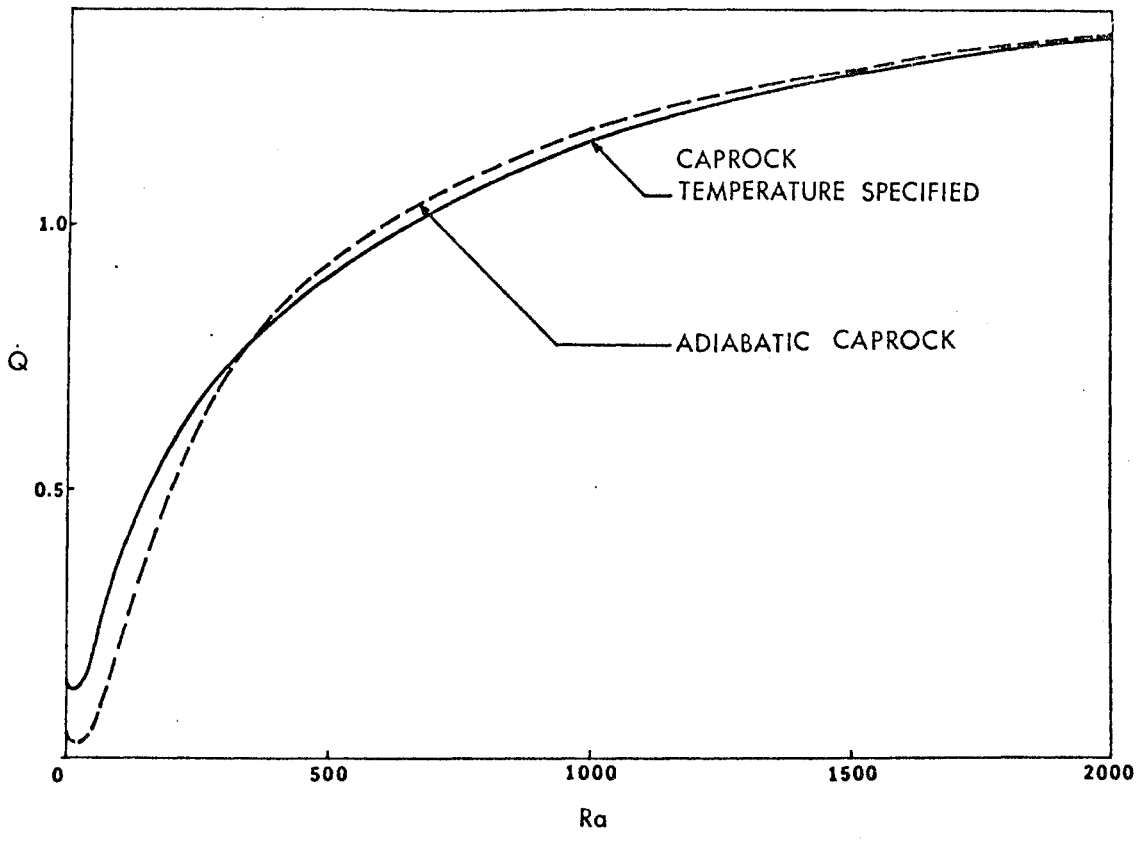

Fig. 13 The Effect of Thermal Boundary Condition at the Caprock on Total Heat Transfer Rate at the Bottom Impermeable Surface

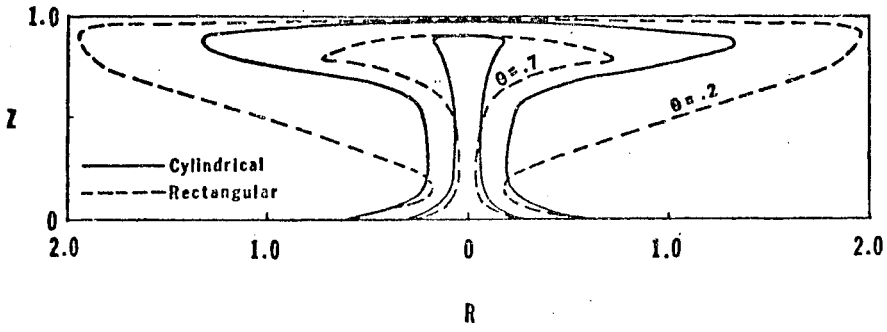

Fig. 14 The Effect of Geometry of the Reservoir on the Isotherms

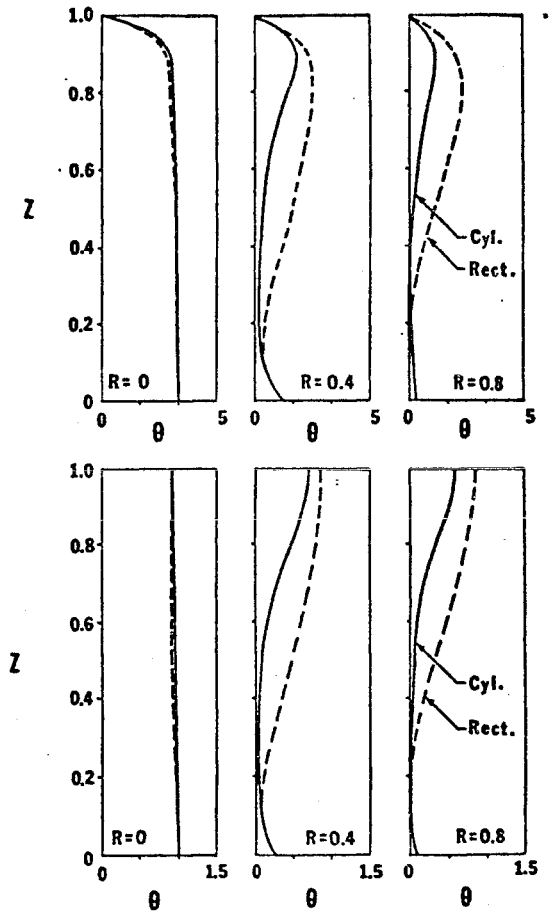

Fig. 15 The Effect of Geometry of the Reservoir on the Vertical Temperature Profiles

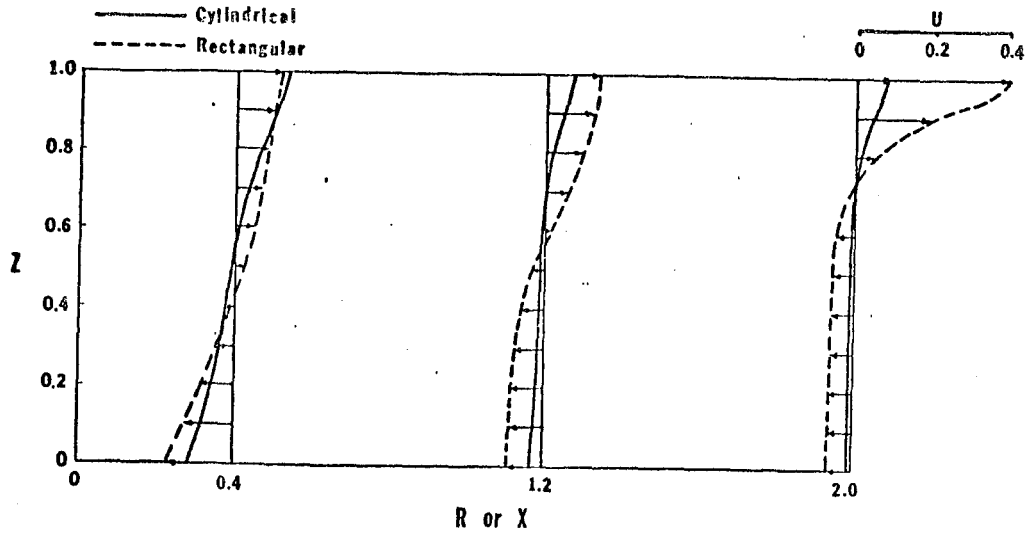

Fig. 16 The Effect of Geometry of the Reservoir on the Horizontal Velocity Distribution

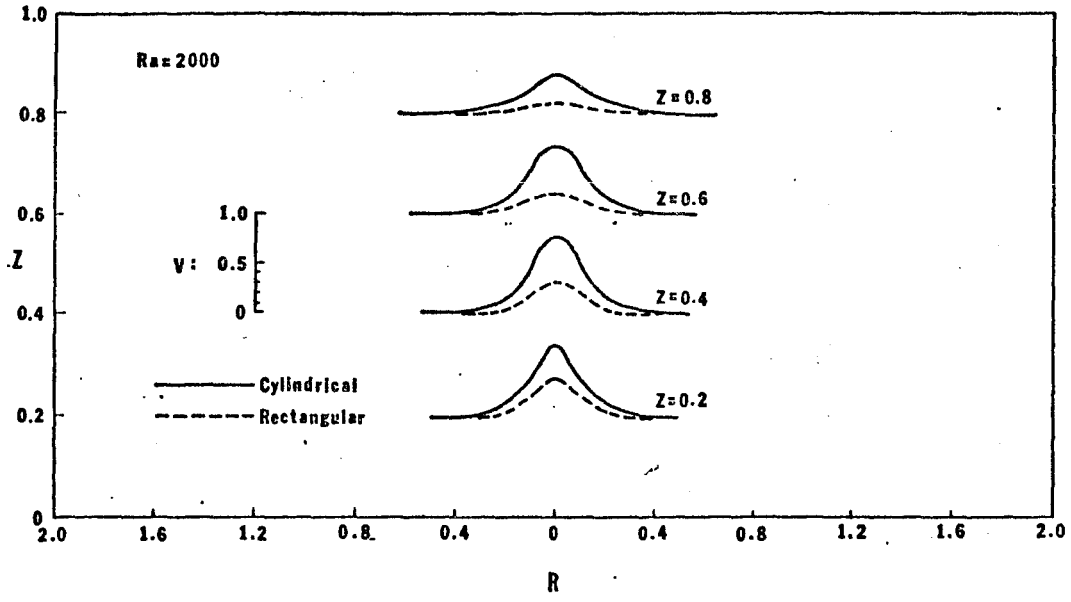

Fig. 17 The Effect of Geometry of the Reservoir on the Vertical Velocity Profiles

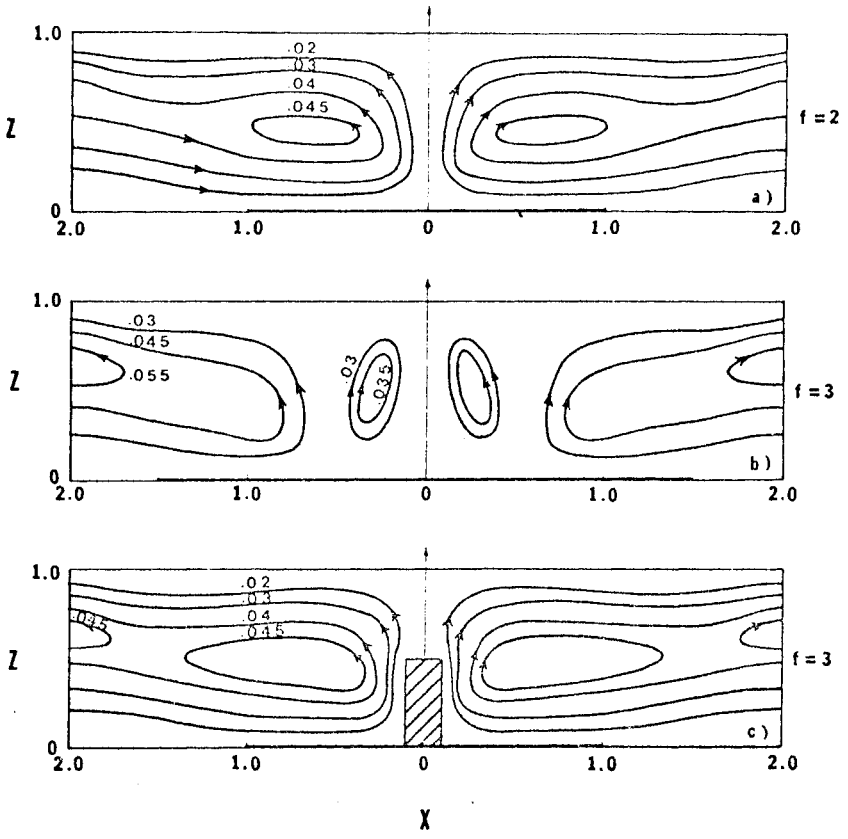

Fig. 18 The Effects of Heating Length and Magmatic Intrusion on Streamlines in a Rectangular Reservoir with Heat-Conducting Caprocks

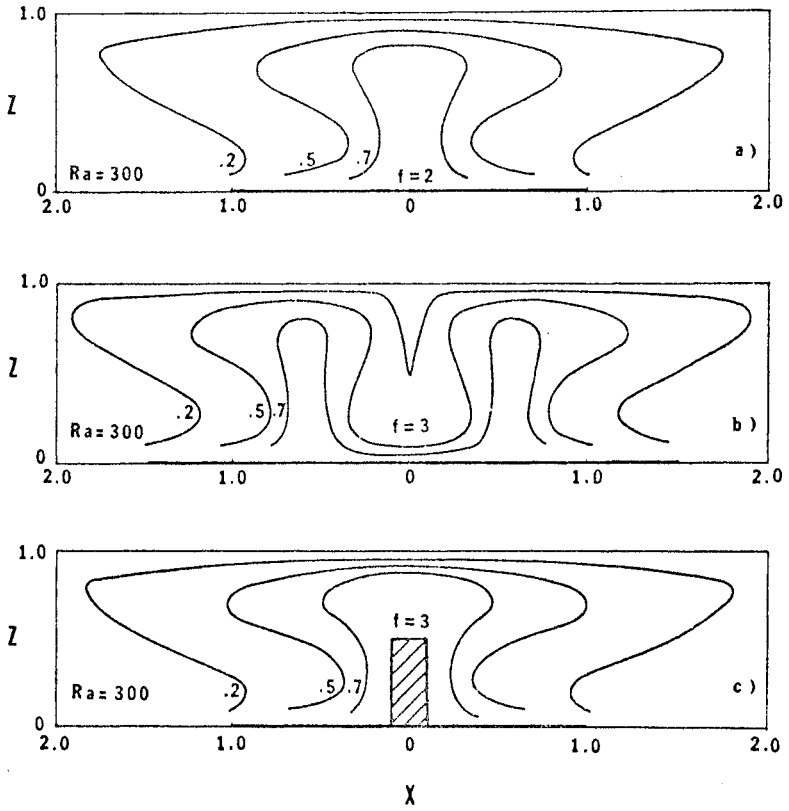

Fig. 19 The Effects of Heating Length and Magmatic Intrusion on the Isotherms in a Rectangular Reservoir with Heat-Conducting Caprocks